AIAA JOURNAL
Vol. 36, No. 11, November 1998

Efficient Approach for Analysis of Unsteady Viscous Flows in Turbomachines

L. He* and W. Ning†
University of Durham, Durham DH1 3LE, England, United Kingdom

A nonlinear harmonic methodology has been developed to calculate unsteady viscous flows through turbomachinery blades. Flow variables are decomposed into time-averaged variables and unsteady perturbations, resulting in the time-averaged equations with extra nonlinear stress terms depending on the unsteady perturbations. An efficient evaluation of an unsteady flowfield is obtained by solving the first-order harmonic equations. The nonlinear interactions between the time-averaged flowfield and the unsteady perturbations were included by a strong coupling approach. The basic computational methodology was applied to the two-dimensional Navier–Stokes equations, and the method was validated against several test cases. Computational results show that this method is much more efficient than the nonlinear time-marching methods while still modeling dominant nonlinear effects.

Nomenclature

A	= computational cell area
f	= physical frequency
N_p	= number of unsteady disturbances
P_b	= exit static pressure
P_0	= inlet stagnation pressure
Re_{δ^*}	= Reynolds number based on boundary-layer displacement thickness
t'	= pseudotime
$\bar{\boldsymbol{U}}$	= vector of time-averaged conservative variables
$\boldsymbol{U}'$	= vector of unsteady perturbation to time-averaged variables
$\tilde{\boldsymbol{U}}$	= vector of complex amplitudes of unsteady perturbations
$\boldsymbol{V}_x$, $\boldsymbol{V}_y$	= viscous flux vectors
ε	= nondimensional amplitude
σ	= interblade phase angle
ϕ	= relative phase angle

I. Introduction

THE development and application of computational fluid dynamics (CFD) have made a significant impact on current design of fluid machinery. The CFD methods for steady flow analysis can now be routinely used in design on a daily basis. In recent years, there has also been considerable progress made in developing and applying CFD methods to predicting unsteady flow phenomena to improve aerodynamic performances and mechanical integrity of turbomachines.

It is known that, for periodic unsteady flows, time averaging results in extra stress terms in the time-averaged equations due to nonlinearity, as formulated in the framework by Adamczyk.[1] Under certain conditions, these nonlinear stress terms might affect both the time-averaged aerodynamic performance and aeroelastic characteristics of blades. The nonlinear effect can be naturally included in the solutions by using conventional nonlinear time-domain integration, e.g., time-marching, methods. Many efforts have been made to use the nonlinear time-marching approach to calculating unsteady flows for blade row interactions[2–4] and blade flutter.[5,6] It is well recognized that the computing resources required by unsteady nonlinear time-marching solutions are much larger than that required by their counterparts for steady flows. One of the main factors is the difficulty in realizing a solution in a single blade-to-blade passage domain. For both blade flutter and rotor/stator interaction problems, periodic unsteadiness would normally be in a circumferentially traveling-wave mode. A phase-shifted periodicity can then be assumed. Several phase-shifted periodic condition methods were proposed to enable solution of a single-passage domain.[2,4,6] However, these methods are subject to various limitations and are not widely used. Consequently, most of the current time-marching computational methods use a multiple-passage (even the whole annulus) domain. The multipassage nonlinear computations have provided very useful research tools for analysis of unsteady flow effects.[7,8] However, because of the large computing resources required, the time-domain multiple-passages solution methods would be too expensive to be used for design purposes. This would probably remain to be the case for some time to come.

The harmonic frequency-domain methods, on the other hand, are computationally much more efficient. There has been continuous development in this area, mainly for blade flutter analysis, e.g., using the potential flow model[9,10] and the Euler equations.[11,12] All of the previous harmonic methods adopt the linear assumption, so that the nonlinear interaction between unsteady disturbances and the time-averaged flow is completely neglected, and consequently, the time-averaged flow must be the same as the steady flow. From a designer's point of view, it seems highly desirable that a method should be developed that takes the advantage of high computing efficiency of the time-linear harmonic approach while including the nonlinear effect of the time-marching method. A stimulating framework of developing such a method was proposed by Giles,[13] based on an asymptotic theory. Following a relatively simple coupling methodology proposed by He,[14] a nonlinear harmonic method was developed and applied to the quasi-three-dimensional inviscid Euler analysis of unsteady flows around oscillating blades by Ning and He.[15] The present work was carried out to deal with the Navier–Stokes analysis of unsteady two-dimensional viscous flows by using the nonlinear harmonic method. In the following sections, the flow models, solution methods, and numerical results will be described.

II. Time-Averaged and Unsteady Flow Models

Basic Unsteady Flow Governing Equations

Consider the two-dimensional Reynolds averaged unsteady Navier–Stokes equations over a finite area ΔA. For simplicity of presentation, we consider that the computational cells are fixed in time. The formulations for moving grids can be found in previous papers.[6,15] The integral form of the equations is

$$\frac{\partial}{\partial t}\iint_{\Delta A} \boldsymbol{U}\,\mathrm{d}A + \oint_S [\boldsymbol{F}\,\mathrm{d}y + \boldsymbol{G}\,\mathrm{d}x] = \oint_S [\boldsymbol{V}_x\,\mathrm{d}y + \boldsymbol{V}_y\,\mathrm{d}x] \tag{1}$$

where

$$\boldsymbol{U} = \begin{bmatrix} \rho \\ \rho u \\ \rho v \\ \rho e \end{bmatrix}, \quad \boldsymbol{F} = \begin{bmatrix} \rho u \\ \rho u u + P \\ \rho u v \\ (\rho e + P)u \end{bmatrix}, \quad \boldsymbol{G} = \begin{bmatrix} \rho v \\ \rho u v \\ (\rho v v + P) \\ (\rho e + P)v \end{bmatrix} \tag{2}$$

Received July 29, 1997; revision received June 25, 1998; accepted for publication July 18, 1998.

*Reader in Turbomachinery Aerodynamics, School of Engineering.
†Ph.D. Graduate Student, School of Engineering; currently Senior Design Engineer, European Gas Turbines, Lincoln LN2 5DJ, England, United Kingdom.

here $\boldsymbol{V}_x$ and $\boldsymbol{V}_y$ are the viscous terms

$$\boldsymbol{V}_x = \begin{bmatrix} 0 \\ \tau_{xx} \\ \tau_{xy} \\ -q_x + u\tau_{xx} + v\tau_{xy} \end{bmatrix}, \qquad \boldsymbol{V}_y = \begin{bmatrix} 0 \\ \tau_{xy} \\ \tau_{yy} \\ -q_y + u\tau_{xy} + v\tau_{yy} \end{bmatrix} \tag{3}$$

where

$$\tau_{xx} = \frac{2}{3}\mu\left(2\frac{\partial u}{\partial x} - \frac{\partial v}{\partial y}\right), \qquad \tau_{yy} = \frac{2}{3}\mu\left(2\frac{\partial v}{\partial y} - \frac{\partial u}{\partial x}\right)$$

$$\tau_{xy} = \mu\left(\frac{\partial u}{\partial y} + \frac{\partial v}{\partial x}\right), \qquad q_x = -k\frac{\partial T}{\partial x}, \qquad q_y = -k\frac{\partial T}{\partial y}$$

$$\mu = \mu_l + \mu_t$$

The laminar flow viscosity μ_l is obtained from Sutherland's law. For a periodically varying unsteady flow, Reynolds averaging can be regarded as an ensemble averaging. It is assumed that the essentially random turbulence can be treated as that in a steady flow, which is accounted for by the turbulent flow viscosity μ_t. Here we use the standard Baldwin–Lomax[16] mixing length model.

Time-Averaged Equations

An unsteady flowfield is decomposed into two parts: a time-averaged flow plus an unsteady perturbation, e.g.,

$$\boldsymbol{U} = \bar{\boldsymbol{U}} + \boldsymbol{U}' \tag{4}$$

Substituting the preceding expression for the conservative variables into the integral form of the unsteady Navier–Stokes equations and time averaging them, the resultant time-averaged equations are given as

$$\oint_s [\bar{\boldsymbol{F}}\,\mathrm{d}y + \bar{\boldsymbol{G}}\,\mathrm{d}x] = \oint_s [\bar{\boldsymbol{V}}_x\,\mathrm{d}y + \bar{\boldsymbol{V}}_y\,\mathrm{d}x] \tag{5}$$

where

$$\bar{\boldsymbol{F}} = \begin{bmatrix} \overline{\rho u} \\ \bar{u}\overline{\rho u} + \bar{P} + \overline{(\rho u)'u'} \\ \bar{v}\overline{\rho u} + \overline{(\rho u)'v'} \\ \bar{H}\overline{\rho u} + \overline{H'(\rho u)'} \end{bmatrix}, \qquad \bar{\boldsymbol{G}} = \begin{bmatrix} \overline{\rho v} \\ \bar{u}\overline{\rho v} + \overline{(\rho v)'u'} \\ \bar{v}\overline{\rho v} + \overline{(\rho v)'v'} \\ \bar{H}\overline{\rho v} + \overline{H'(\rho v)'} \end{bmatrix} \tag{6}$$

$$\bar{\boldsymbol{V}}_x = \begin{bmatrix} 0 \\ \bar{\tau}_{xx} \\ \bar{\tau}_{xy} \\ -\bar{q}_x + \bar{u}\bar{\tau}_{xx} + \bar{v}\bar{\tau}_{xy} + \overline{u'\tau'_{xx}} + \overline{v'\tau'_{xy}} \end{bmatrix}$$

$$\bar{\boldsymbol{V}}_y = \begin{bmatrix} 0 \\ \bar{\tau}_{xy} \\ \bar{\tau}_{yy} \\ -\bar{q}_y + \bar{u}\bar{\tau}_{xy} + \bar{v}\bar{\tau}_{yy} + \overline{u'\tau'_{xy}} + \overline{v'\tau'_{yy}} \end{bmatrix} \tag{7}$$

Comparison between the time-averaged equations and the steady form of the original unsteady equations shows that the time averaging generates extra terms in the momentum and energy equations due to nonlinearity. These extra terms are similar to the turbulence (Reynolds) stress terms and can be called unsteady stress terms. Care should also be taken when calculating nonconservative variables. For instance, the time-averaged axial velocity is worked out by

$$\bar{u} = \frac{\overline{\rho u} - \overline{\rho' u'}}{\bar{\rho}}$$

For the present work, it is assumed that both the laminar and turbulence viscosity coefficients are frozen during time averaging, i.e., unaffected by unsteady flows. As a result, the viscous terms are in a linear form except for those concerning the work done by viscous stresses in the energy equation. It is recognized that the nonlinearity of turbulence and its behavior in the Reynolds averaged equations could well be turbulence-model specific and might interact with the nonlinear effects of periodic unsteadiness. Further investigations into the treatment of turbulence should be carried out in the future.

Unsteady Perturbation Equations and Harmonic Formulations

The equations for unsteady perturbations can be obtained by the difference between the basic unsteady flow equations [Eq. (1)] and the time-averaged equations [Eq. (5)]. But this complete form of the unsteady perturbation equations is not readily solvable if a frequency-domain approach is to be used. It is further assumed that the unsteady perturbations are dominated by the first-order terms. Therefore, the unsteady perturbation equations can be formed by collecting all of the first-order terms from the basic unsteady flow equations, which gives

$$\frac{\partial}{\partial t}\iint_{\Delta A} \boldsymbol{U}'\,\mathrm{d}A + \oint_s [(\boldsymbol{F}' - \boldsymbol{V}'_x)\,\mathrm{d}y + (\boldsymbol{G}' - \boldsymbol{V}'_y)\,\mathrm{d}x] = 0 \tag{8}$$

where

$$\boldsymbol{F}' = \begin{bmatrix} (\rho u)' \\ u'\overline{\rho u} + \bar{u}(\rho u)' + P' \\ \overline{\rho v}u' + (\rho v)'\bar{u} \\ H'\overline{\rho u} + \bar{H}(\rho u)' \end{bmatrix}, \qquad \boldsymbol{G}' = \begin{bmatrix} (\rho v)' \\ u'\overline{\rho v} + \bar{u}(\rho v)' \\ \overline{\rho v}v' + (\rho v)'\bar{v} \\ H'\overline{\rho v} + \bar{H}(\rho v)' \end{bmatrix}$$

$$\boldsymbol{V}'_x = \begin{bmatrix} 0 \\ \tau'_{xx} \\ \tau'_{xy} \\ -q'_x + \bar{u}\tau'_{xx} + \bar{v}\tau'_{xy} + u'\bar{\tau}_{xx} + v'\bar{\tau}_{xy} \end{bmatrix}$$

$$\boldsymbol{V}'_y = \begin{bmatrix} 0 \\ \tau'_{xy} \\ \tau'_{yy} \\ -q'_y + \bar{u}\tau'_{xy} + \bar{v}\tau'_{yy} + u'\bar{\tau}_{xy} + v'\bar{\tau}_{yy} \end{bmatrix}$$

The unknowns of the unsteady equations are the perturbations to the conservative variables. Other variables are obtained by linearized relations, e.g.,

$$u' = \frac{(\rho u)' - \bar{u}\rho'}{\bar{\rho}}$$

The resultant unsteady perturbation equations are in a quasilinear form, i.e., the perturbations are linear for a given time-averaged flowfield. Indeed, if the time-averaged flow is the same as the steady flow, the preceding unsteady perturbation equations are reduced to the conventional linear perturbation equations.

At this stage, we can introduce a harmonic temporal variation for an unsteady perturbation. For general situations of periodic unsteady flows in turbomachines, a flowfield may be subject to multiple disturbances of the form[17]

$$\boldsymbol{U} = \bar{\boldsymbol{U}} + \sum_{i=1}^{N_p} \boldsymbol{U}'_i \tag{9}$$

where N_p is the total number of unsteady disturbances. Each disturbance is characterized by its own frequency and interblade phase angle and can be approximated by the Fourier series. For a nonlinear time-domain solution, time averaging of the unsteady flow with multiple disturbances will have to be carried out over a period when all disturbances beat. On the other hand, the linear nature of the first-order perturbation equations means that all of the disturbances and their harmonics can be solved separately. Their contributions to the time-averaged flows can be easily evaluated due to the orthogonal property of trigonometric functions. For instance, consider that unsteady velocity perturbations can be decomposed into the disturbances with N_p distinctive frequencies:

$$u' = \sum_{i=1}^{N_p} u'_i, \qquad v' = \sum_{i=1}^{N_p} v'_i$$

The nonlinear stress terms are simply a summation of the products for each frequency, e.g.,

$$\overline{u'v'} = \sum_{i=1}^{N_p} \overline{u'_i v'_i}$$

Thus, the general formulation [Eq. (9)] can include all significant harmonic components as long as the corresponding harmonic

boundary conditions can be specified. However, the adoption of the first-order equations implies that the nonlinear interaction between different disturbances with different frequencies would only be included by communicating with the time-averaged flow.

Without loss of generality, the work presented in the rest of this paper considers only one periodic disturbance in its first harmonic form, i.e.,

$$\boldsymbol{U}' = \tilde{\boldsymbol{U}}\, e^{i\omega t}$$

The resultant first-order harmonic perturbation equations can be written as

$$\oint_s [(\tilde{\boldsymbol{F}} - \tilde{\boldsymbol{V}}_y)\,\mathrm{d}y + (\tilde{\boldsymbol{G}} - \tilde{\boldsymbol{V}}_x)\,\mathrm{d}x] = -i\omega \iint_{\Delta A} \tilde{\boldsymbol{U}}\,\mathrm{d}A \tag{10}$$

All of the parameters in Eq. (10) are space dependent only because the equations are cast in the frequency domain.

III. Solution Method

Pseudotime Dependence and Spatial Discretization

To make use of the efficient time-marching integration schemes extensively developed for steady flows, a pseudotime variable t' is introduced to the first-order harmonic perturbation equations, as proposed by Ni and Sisto[18] for conventional linear methods. A pseudotime dependence is also included in the time-averaged flow equations, similar to the conventional steady flow time-marching solvers. Using this technique, the time-averaged equations and the first-order harmonic perturbation equations become

$$\frac{\partial}{\partial t'} \iint_{\Delta A} \bar{\boldsymbol{U}}\,\mathrm{d}A + \oint_s [(\bar{\boldsymbol{F}} - \bar{\boldsymbol{V}}_x)\,\mathrm{d}y + (\bar{\boldsymbol{G}} - \bar{\boldsymbol{V}}_y)\,\mathrm{d}x] = 0 \tag{11}$$

and

$$\frac{\partial}{\partial t'} \iint_{\Delta A} \tilde{\boldsymbol{U}}\,\mathrm{d}A + \oint_s [(\tilde{\boldsymbol{F}} - \tilde{\boldsymbol{V}}_y)\,\mathrm{d}y + (\tilde{\boldsymbol{G}} - \tilde{\boldsymbol{V}}_x)\,\mathrm{d}x] = -i\omega \iint_{\Delta A} \tilde{\boldsymbol{U}}\,\mathrm{d}A \tag{12}$$

Now both the time-averaged and the unsteady perturbation equations are hyperbolic in time. Because only the steady-state solutions are desired, all of the standard steady flow acceleration methods, such as the local time stepping and the multiple grid acceleration techniques, can be used to accelerate computations.

The spatial discretization for the equations is made by using the cell-vertex finite volume scheme. Consider an H mesh consisting of $I \times J$ quadrilateral cells. For each mesh cell, Eqs. (11) and (12) can be written in a semidiscrete form, e.g., for a cell with an index (i, j),

$$\frac{\mathrm{d}}{\mathrm{d}t'}(\bar{\boldsymbol{U}}\Delta A)_{ij} = (\bar{\boldsymbol{F}}_I + \bar{\boldsymbol{F}}_V)_{ij} \tag{13}$$

$$\frac{\mathrm{d}}{\mathrm{d}t'}(\tilde{\boldsymbol{U}}\Delta A)_{ij} = (\tilde{\boldsymbol{F}}_I + \tilde{\boldsymbol{F}}_V)_{ij} \qquad (i = 1, 2, \ldots, I;\ j = 1, 2, \ldots, J) \tag{14}$$

where

$$\bar{F}_I = -\sum_1^4 [\bar{F}\Delta y + \bar{G}\Delta x], \qquad \bar{F}_V = \sum_1^4 [\bar{V}_x \Delta y + \bar{V}_y \Delta x]$$

$$\tilde{F}_I = -\sum_1^4 [\tilde{F}\Delta y + \tilde{G}\Delta x] - i\omega\tilde{\boldsymbol{U}}\Delta A$$

$$\tilde{F}_V = \sum_1^4 [\tilde{V}_x \Delta y + \tilde{V}_y \Delta x]$$

The summation is taken along the four boundary surfaces of the cell. The fluxes across each surface are evaluated using the flow variables stored at the corners of the cell. For viscous fluxes, the first-order spatial derivatives are evaluated by using the Gauss theorem on auxiliary cells.[19] Once the temporal change is evaluated, it is equally distributed to the four corners of the cell.

To suppress numerical oscillations and capture the shock waves in the time-averaged flow and the shock impulse in the first-order perturbations, second- and fourth-order adaptive smoothing[20] is used in both the streamwise and the pitchwise directions. It is recognized that the pressure sensor in the original numerical damping for shock capturing would act in a nonlinear manner, and this nonlinear effect on the time-averaged and unsteady perturbations needs to be included. In the present work, an approximate formulation is used based on a simple analysis of the time-averaging effect on a time-averaged damping coefficient to linearize the pressure sensor. Consider a pressure sensor in the x direction in the form

$$\nu_i = \left| \frac{P_{i+1} - 2P_i + P_{i-1}}{P_{i+1} + 2P_i + P_{i-1}} \right| \tag{15}$$

Its time-averaged counterpart will be

$$\overline{\nu_i} = \left| \frac{\overline{P_{i+1}} - 2\overline{P_i} + \overline{P_{i-1}}}{\overline{P_{i+1}} + 2\bar{P}_i + \overline{P_{i-1}}} \right| + 0.5 \left| \frac{\tilde{P}_{i+1} - 2\tilde{P}_i + \tilde{P}_{i-1}}{\overline{P_{i+1}} + 2\bar{P}_i + \overline{P_{i-1}}} \right| \tag{16}$$

Coupling Between Time-Averaged and Unsteady Flows

Because of the physical nature of the interaction between the time-averaged flow and the unsteady disturbances, the time-averaged equations and the unsteady perturbation equations are interdependent. A coupled-solution method would, therefore, need to be considered. Based on the past experience with inviscid–viscous coupling and fluid-structure coupling, it was decided to adopt the simultaneous time-marching procedure. This is an easy procedure to implement, and because of its strong coupling nature, it provides a fast convergence rate and high stability, which might be significant when the interaction between two parts becomes strong. The entire coupled system consisting of the two sets of equations is integrated simultaneously in time by using the four-stage Runge–Kutta scheme. The formulations of the four-stage Runge–Kutta scheme from time step n to $n+1$ are

$$(\bar{\boldsymbol{U}})_{ij}^{n+\alpha_k} = (\bar{\boldsymbol{U}})_{ij}^{n} + \alpha_k \frac{\Delta t'}{\Delta A} (\bar{\boldsymbol{F}}_I + \bar{\boldsymbol{F}}_V)_{ij}^{n+\alpha_{k-1}} \tag{17a}$$

$$(\tilde{\boldsymbol{U}})_{ij}^{n+\alpha_k} = (\tilde{\boldsymbol{U}})_{ij}^{n} + \alpha_k \frac{\Delta t'}{\Delta A} (\tilde{\boldsymbol{F}}_I + \tilde{\boldsymbol{F}}_V)_{ij}^{n+\alpha_{k-1}} \qquad (i = 1, 2, \ldots, I;\ j = 1, 2, \ldots, J) \tag{17b}$$

where $k = 1$–4 for the four-stage Runge–Kutta integration and

$$\alpha_0 = 0, \qquad \alpha_1 = \tfrac{1}{4}, \qquad \alpha_2 = \tfrac{1}{3}, \qquad \alpha_3 = \tfrac{1}{2}, \qquad \alpha_4 = 1$$

For solving the time-averaged equations, the unsteady stress terms need extra relationships to be closed. For a periodically unsteady flow, the unsteady stress terms can be directly evaluated in terms of the phase and amplitude of the perturbations. For example, u' and v' are two unsteady quantities changing in the harmonic form, and the time averaging of $u'v'$ over one oscillating period is

$$\overline{u'v'} = \tfrac{1}{2} A_{mu} A_{mv} \cos(\phi_{vu}) \tag{18}$$

where A_{mu} and A_{mv} are the amplitudes of u' and v' and ϕ_{vu} is the relative phase angle between u' and v'.

Boundary Conditions

A single blade-to-blade passage domain is adopted. Boundary conditions are required for inlet/exit, periodic, and blade surface boundaries. Given an interblade phase angle σ, the phase-shift periodic condition is easily implemented by

$$(\tilde{\boldsymbol{U}})^U = (\tilde{\boldsymbol{U}})^L\, e^{i\sigma}$$

where superscripts U and L denote the flow variables at the upper and lower periodic boundaries. For the inlet/exit conditions, the conventional method of specifying the inlet stagnation pressure, stagnation temperature, flow angle, and outlet static pressure is used for the time-averaged equations. For the first-order harmonic perturbation equations, the two-dimensional nonreflecting boundary condition for a single-frequency unsteady flow[21] is adopted.

On the solid wall, two different conditions can be used. The first one is the no-slip wall condition, in which the time-averaged velocities and perturbation velocities are set to zero on the wall. The second method is to set the time-averaged and perturbation wall shear stresses and to allow the time-averaged velocities and perturbation velocities to slip. An approximate form of the log law[22] is used to calculate the time-averaged wall shear stress. The perturbation wall shear stress is obtained by linearizing the approximate

log law. For the cases presented later, the slip wall condition with the linearized log law was used, except for the unsteady boundary layer cases, where much finer meshes were used and the nonslip wall condition was applied.

One issue concerning the solid surface boundary condition should be mentioned. Because some linearized Euler methods have been already developed, it would seem to be practically beneficial if these linearized Euler methods can be directly applied, based on a steady base flowfield provided by a separate well-developed steady viscous flow solver. The question is, can we solve the unsteady inviscid Euler perturbation equations based on a steady viscous flowfield provided by a Navier–Stokes solver? Numerical tests were carried out to address this issue by switching off all of the viscous perturbation terms and running the resultant inviscid Euler perturbation equations based on a steady viscous flowfield, using the same mesh. The present test results show that, for some cases, the harmonic Euler perturbation method with the pure slip wall condition, i.e., without any constraint on the tangential velocity, revealed serious convergence problems. This might be because the original unsteady viscous flow model requires that the tangential velocity must be constrained either by the nonslip wall condition or by the applied wall shear stress. This constraint would be effectively lost if the inviscid Euler (or potential) perturbation equations are used for the unsteady part of the flow, regardless of the condition applied in the steady viscous flow part. Therefore, it seems that both the time-averaged and the unsteady perturbation flow models would have to be either inviscid or viscous.

IV. Computational Results

Unsteady Laminar and Turbulent Boundary Layers on Flat Plate

To validate the basic method, unsteady laminar and turbulent boundary layers on a flat plate were calculated. In the laminar flow case, the main stream velocity fluctuates in the form

$$u = u_0(1 + \varepsilon e^{i\omega t})$$

where u_0 is the mean and constant flow velocity. This model problem was initially analyzed by Lighthill.[23] In the present study, the unsteady laminar flow through a low-speed channel ($M \sim 0.1$), in which there are approximately 25 mesh points across the boundary layer, was computed. The channel width was chosen to be sufficiently large so that the boundary-layer blockage effect was negligible. Figures 1 and 2 show the variations of calculated wall shear stress amplitudes and phase angles. The results are in satisfactory agreement with Lighthill's analytic results for both low and high frequencies, as well as with Cebeci's[24] numerical solution.

The turbulent flow case was experimentally studied by Karlsson.[25] In the experiment, an oscillating unsteady boundary layer under a zero mean streamwise pressure gradient was measured at a Reynolds number of $Re_{\delta^*} = 3.6 \times 10^3$. In the present study, the unsteady flow was simulated by prescribing an unsteady perturbation pressure at the exit. The computations were carried out to match the experimental Reynolds number and the reduced frequencies corresponding to two experimental frequency conditions ($f = 0.33$ and 1 Hz). A comparison between the calculated time-averaged velocity profile and the experimental data is shown in Fig. 3. Figure 4 shows

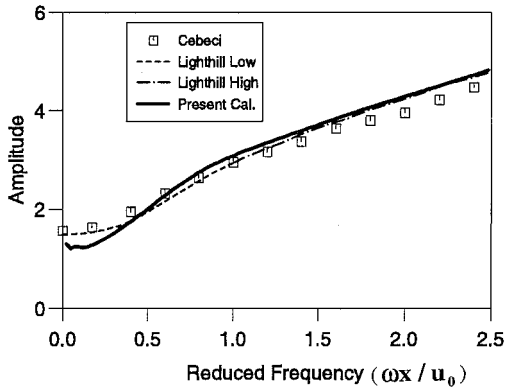

Fig. 1 Amplitude of the wall shear fluctuations for an oscillating laminar boundary layer.

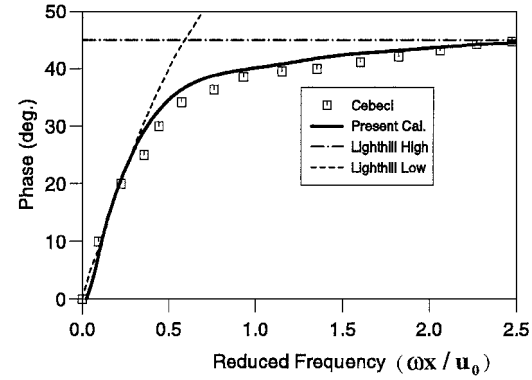

Fig. 2 Phase angle between wall shear and external velocity for an oscillating laminar boundary layer.

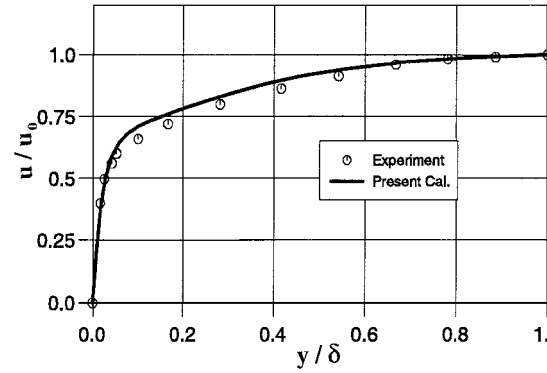

Fig. 3 Time-averaged velocity profiles for an oscillating turbulent boundary layer.

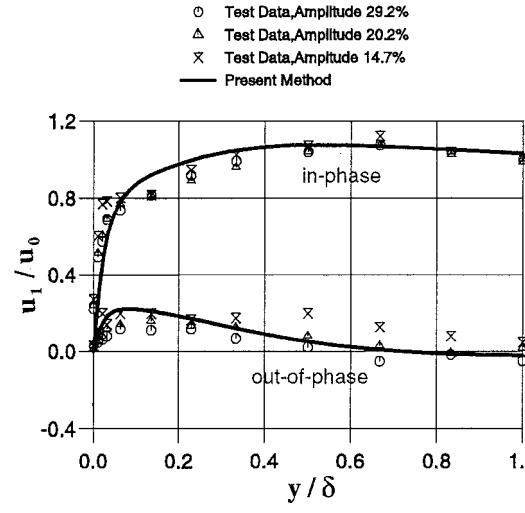

f = 0.33 Hz

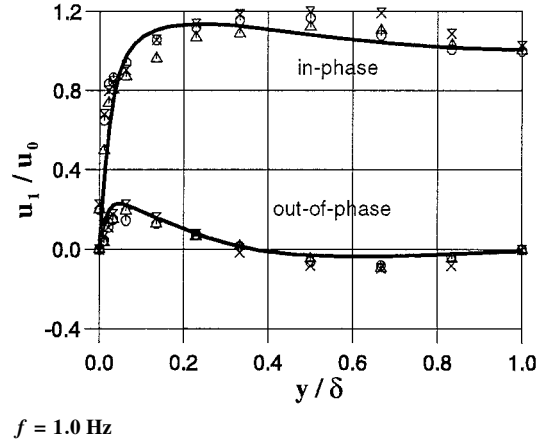

f = 1.0 Hz

Fig. 4 In-phase and out-of-phase velocity components for an oscillating turbulent boundary layer.

the comparison between calculated and experimental values of the in-phase and out-of-phase components of perturbation velocities, respectively. The present calculated results are in good agreement with the experimental data. For both the laminar and the turbulent boundary-layer cases, the present computational results show little nonlinear effect.

Transonic Diffuser with Oscillating Back Pressure

This case was experimentally studied by Sajben et al.[26] The computations were carried out with a back pressure ratio P_b/P_0 of 0.826, producing a weak shock with a preshock Mach number of 1.24 at $x/h^* = 1.4$, where x is the streamwise distance measured from the throat and h^* the throat height. The Reynolds number, based on h^* and stagnation conditions at the inlet, is 1.1×10^6. The calculations were carried out assuming fully turbulent boundary layers on both the top and bottom walls.

A computational mesh with a density of 122×45 cells (Fig. 5) was used. The steady Mach number contours are presented in Fig. 6. The calculated steady pressure distribution along the top wall is shown in Fig. 7. The experimental shock position and strength are well predicted by the present steady viscous calculation. The marked difference between the steady viscous and inviscid solutions indicates a significant boundary-layer blockage effect.

In the experiment, the forced back pressure oscillation was induced by rotating a triangular bar, and unsteady pressure distributions downstream of the shock wave were measured. Calculations were carried out with the exit harmonic pressure oscillation at a frequency of $f = 150$ Hz. Three methods were used: the nonlinear harmonic method, the linear method, and the fully nonlinear time-marching method.

The amplitude and phase distributions of the unsteady pressure are shown in Fig. 8. It can be seen that the linear method overpredicts the peak amplitude of the unsteady shock impulse by a factor of more than 2. The comparison between the present nonlinear harmonic method and the nonlinear time-marching method is very good. Figure 9 shows the time-averaged static pressure distributions obtained by the nonlinear time-marching method and the nonlinear harmonic method. The time-averaged shock wave is smeared by the unsteadiness, and this is well predicted by the present nonlinear harmonic method.

To check the mesh dependence of the present nonlinear harmonic method, a calculation with a fine mesh (245×45) was also carried out. The time-averaged streamwise static pressure distributions using the two meshes are shown in Fig. 10. The corresponding unsteady pressure distributions are given in Fig. 11. The results illustrate that the mesh dependence of the present nonlinear harmonic method is small.

Oscillating Transonic Compressor Cascade

To examine the advantages of using the present nonlinear harmonic method for unsteady flows in turbomachinery, an oscillating compressor cascade was calculated. The cascade is of a biconvex profile with a chord of 0.0762 m, a maximum relative thickness of 2%, and a stagger angle of 59 deg. The cascade flow is subject to an inlet Mach number of 1.25, a Reynolds number of 1.5×10^6, and a back pressure ratio P_b/P_0 of 0.6. The flow is assumed to be fully turbulent from the leading edge. The cascade geometry and flow conditions are typical of tip sections of transonic compressors.

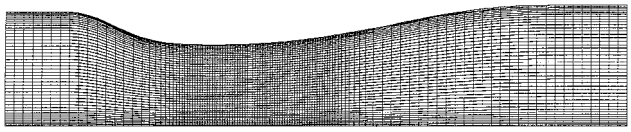

Fig. 5 Computational mesh for a transonic diffuser; mesh size 122 × 45, vertical scale enlarged by a factor of 2.

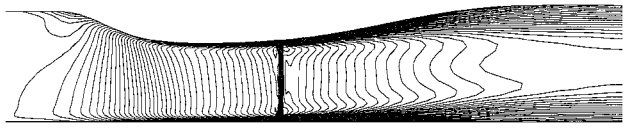

Fig. 6 Mach number contours for a transonic diffuser; vertical scale enlarged by a factor of 2.

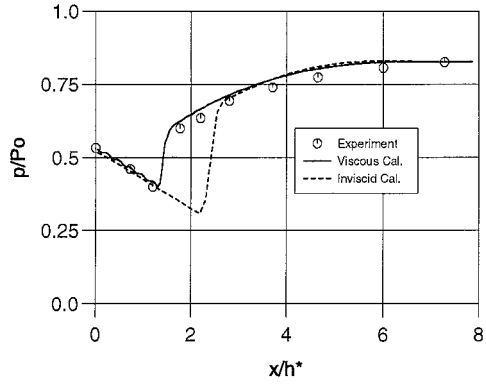

Fig. 7 Steady static pressure on top wall of a transonic diffuser.

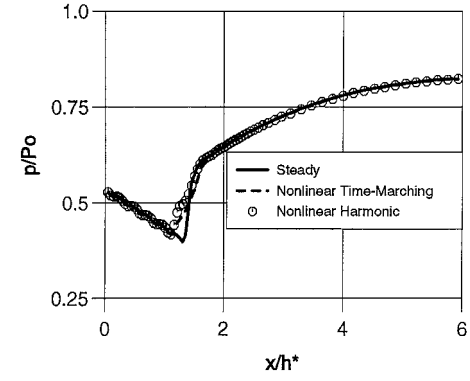

Fig. 9 Steady and time-averaged pressure distributions on top wall of a transonic diffuser.

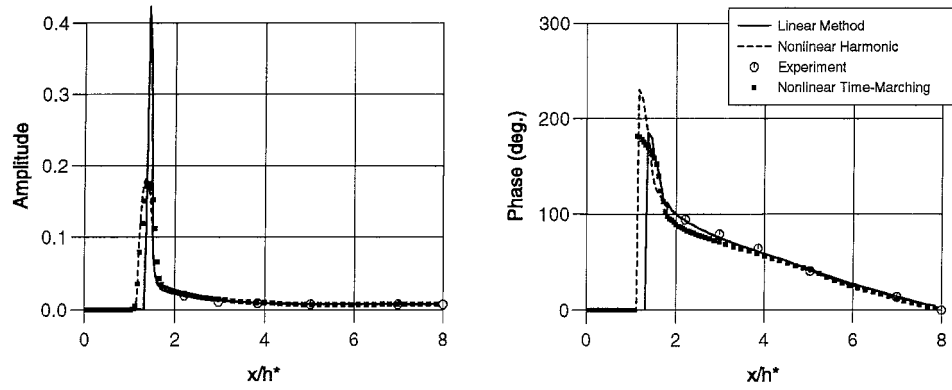

Fig. 8 Amplitude and phase distributions of unsteady pressure on top wall of a transonic diffuser.

The unsteady flow was induced by the blades oscillating in a torsion mode around the midchord with an amplitude of 0.5 deg and a reduced frequency of 0.5. The interblade phase angle is 180 deg. The computation was carried out with a mesh of 115×35 cells per blade passage, as shown in Fig. 12. Again, the calculated results are compared among the pure linear method, the nonlinear harmonic method, and the fully nonlinear time-marching method. For the nonlinear time-marching calculation, a two-passage domain was used with the direct repeating (periodic) boundary condition.

Figure 13 shows the steady surface static pressure distributions. Figure 14 shows the steady Mach number contours. It can be seen that the cascade is subject to a strong passage shock wave, typical of a modern transonic fan at a near peak efficiency condition. The unsteady pressure distributions are shown in Fig. 15. Again the amplitude of unsteady shock impulse captured by the linear method is much higher than that obtained by the nonlinear time-marching method. The results by the present nonlinear harmonic show a considerable improvement over the pure linear method, in terms of both amplitude and phase angle. It should be emphasized that, for a blade oscillation in a torsion mode, a detailed (rather than integral) unsteady loading distribution is important for calculations of blade flutter characteristics.

An examination of mesh dependence was also carried out for this case. Figure 16 shows the unsteady pressure distributions using two meshes: 115×35 and 115×45. The results with the different meshes are in good agreement, suggesting negligible mesh dependence of the nonlinear harmonic method.

Finally, some comments should be made with regard to computing time. For the cascade case, the nonlinear harmonic solution requires 1.5 CPU hours on a single processor of a SGI Power Challenger workstation, which is 60% more than that required by the pure linear solution. This CPU time consumed by the nonlinear harmonic solution is comparable to that by the nonlinear time-marching solution for one blade passage. The point is, a single-passage domain can always be adopted for the nonlinear harmonic method,

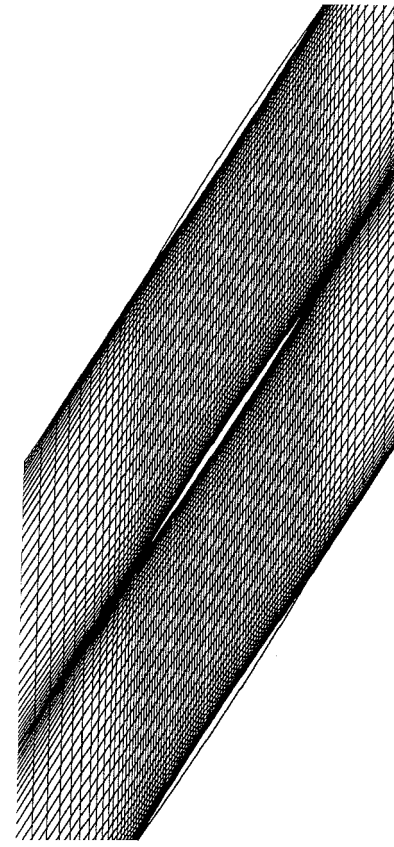

Fig. 12 Computational mesh for a transonic cascade.

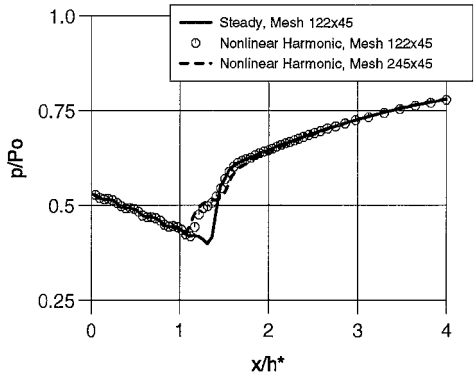

Fig. 10 Steady and time-averaged pressure distributions on top wall of a transonic diffuser with different meshes.

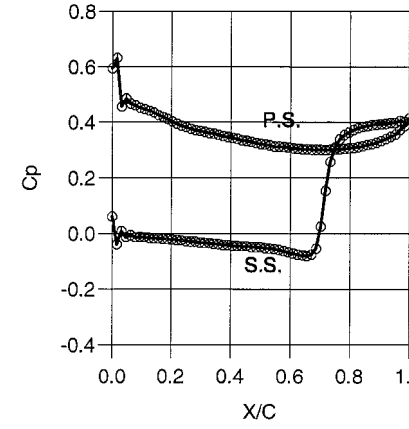

Fig. 13 Calculated steady pressure distributions on blade surfaces for a transonic cascade.

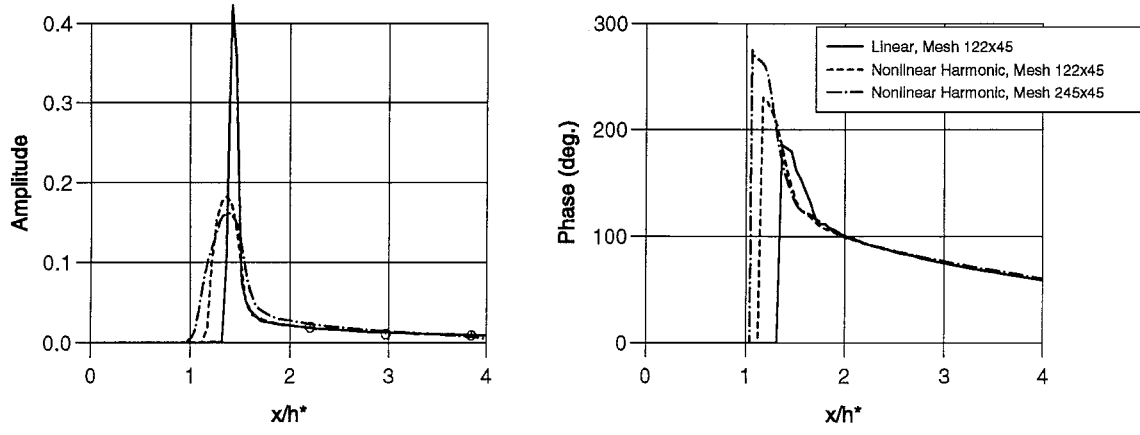

Fig. 11 Unsteady pressure distribution on top wall of a transonic diffuser with different meshes.

whereas a multiple-passage domain has to be adopted by the conventional nonlinear time-marching methods. For a blade flutter case with one nodal-diameter mode, the whole annulus domain has to be used for the time-marching solution. Numerical tests show that, for an annulus with 20 blade passages, the present nonlinear harmonic solution with one harmonic disturbance is about 20 times faster than a 20-passage time-marching solution. Also, we have not yet introduced any acceleration techniques, such as the multiple grid. A further speedup of the nonlinear harmonic solution by a factor of 5 or more would be expected once the multigrid technique is used.

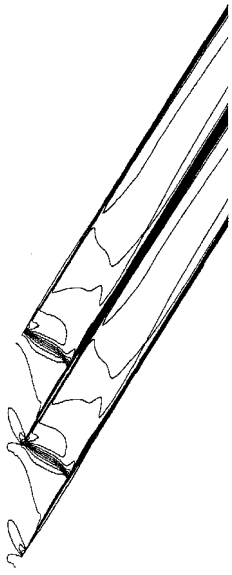

Fig. 14 Calculated Mach number contours for a transonic cascade.

Concluding Remarks

For unsteady turbomachinery flow analysis, the current nonlinear time-domain methods are prohibitively expensive for design purposes, whereas the conventional linearized methods, though computationally very efficient, are limited by the fundamental linear assumption.

A nonlinear harmonic methodology is presented for unsteady viscous flow analysis. It is aimed at taking advantage of the high computing efficiency of the linear methods but to include dominant nonlinear effects. This is achieved by coupling the time-averaged equations and the first-order perturbation equations by a simultaneous pseudotime-marching procedure. Computations with the two-dimensional Navier–Stokes equations and the mixing length turbulence model were carried out to validate the basic algorithm and to examine the effectiveness of the methodology in dealing with nonlinear effects. The numerical studies illustrate that the present nonlinear harmonic method can significantly improve the results over a conventional linear method and is far more efficient than a fully nonlinear time-domain method.

Acknowledgments

This work is sponsored by European Gas Turbines. The authors wish to acknowledge Roger Wells and Yansheng Li for their technical support.

References

[1] Adamczyk, J. J., "Model Equations for Simulating Flows in Multistage Turbomachinery," American Society for Mechanical Engineers, ASME Paper 85-GT-226, June 1985.

[2] Erdos, J. I., Alzner, E., and Mcnally, W., "Numerical Solution of Periodic Transonic Flow Through Fan Stage," *AIAA Journal*, Vol. 15, No. 11, 1977, pp. 1559–1568.

[3] Rai, M. M., "Three-Dimensional Navier–Stokes Simulations of Turbine Rotor–Stator Interaction," *AIAA Journal*, Vol. 5, No. 3, 1989, pp. 305–319.

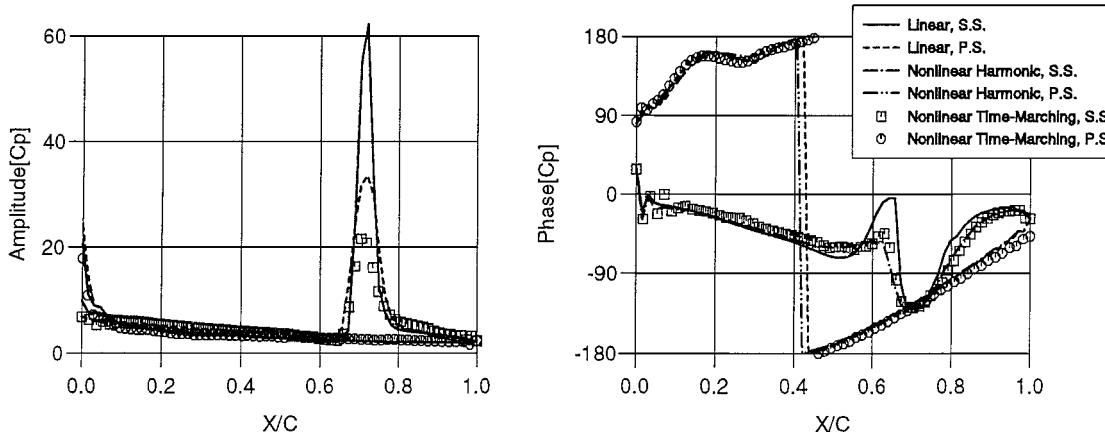

Fig. 15 Amplitude and phase angle distributions of unsteady pressure on blade surfaces.

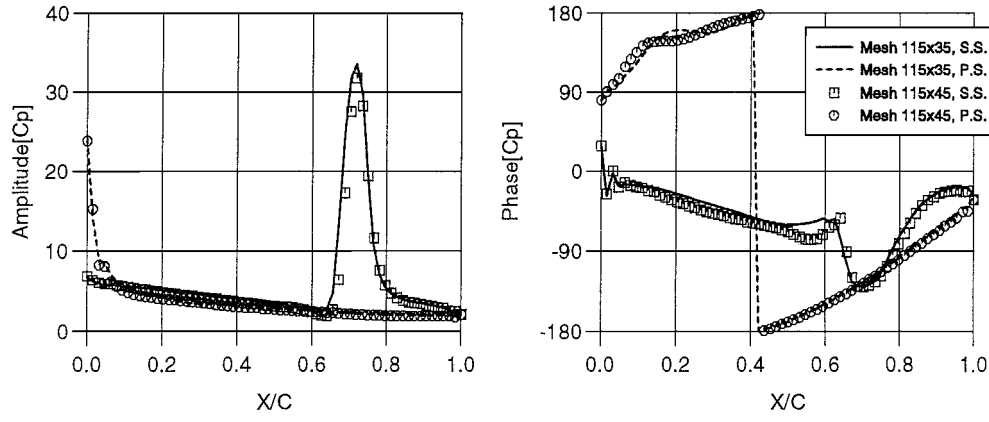

Fig. 16 Unsteady pressure distributions on blade surfaces with different meshes.

[4]Giles, M. B., "Stator/Rotor Interaction in a Transonic Turbine," *Journal of Propulsion and Power*, Vol. 6, No. 5, 1990, pp. 621–627.

[5]Gerolymos, G. A., "Advance in the Numerical Integration of the 3-D Euler Equations in Vibrating Cascades," American Society of Mechanical Engineers, ASME Paper 92-GT-170, June 1992.

[6]He, L., "An Euler Solution for Unsteady Flows Around Oscillating Blades," *Journal of Turbomachinery*, Vol. 112, 1990, pp. 714–722.

[7]Dawes, W. N., "A Numerical Study of the Interaction of a Transonic Compressor Rotor Overtip Leakage Vortex with the Following Stator Blade Row," American Society of Mechanical Engineers, ASME Paper 94-GT-156, June 1994.

[8]Arnone, A., and Pacciani, R., "IGV-Rotor Interaction Analysis in a Transonic Compressor Using the Navier–Stokes Equations," American Society of Mechanical Engineers, ASME Paper 96-GT-141, June 1996.

[9]Whitehead, D. S., "A Finite Element Solution of Unsteady Flow in Cascades," *International Journal for Numerical Methods in Fluids*, Vol. 10, No. 1, 1990, pp. 13–34.

[10]Verdon, J. M., and Caspar, J. R., "A Linearized Unsteady Aerodynamic Analysis for Transonic Cascades," *Journal of Fluid Mechanics*, Vol. 149, 1982, pp. 403–429.

[11]Hall, K. C., and Crawley, E. F., "Calculation of Unsteady Flows in Turbomachinery Using the Linearized Euler Equations," *AIAA Journal*, Vol. 27, No. 6, 1989, pp. 777–787.

[12]Lindquist, D. R., and Giles, M. B., "On the Validity of Linearized Unsteady Euler Equations for Shock Capturing," AIAA Paper 91-1958, 1991.

[13]Giles, M. B., "An Approach for Multi-Stage Calculations Incorporating Unsteadiness," American Society of Mechanical Engineers, ASME Paper 92-GT-282, June 1992.

[14]He, L., "Modelling Issues for Computation of Unsteady Turbomachinery Flows," *Unsteady Flows in Turbomachines*, von Kármán Inst. Lecture Series 1996-05, von Kármán Inst. for Fluid Dynamics, Rhode Saint Genese, Belgium, March 1996.

[15]Ning, W., and He, L., "Computation of Unsteady Flows Around Oscillating Blades Using Linear and Non-Linear Harmonic Euler Methods," *Journal of Turbomachinery*, Vol. 120, No. 3, 1998, pp. 508–514; also American Society of Mechanical Engineers, ASME Paper 97-GT-229, 1997.

[16]Baldwin, B. S., and Lomax, H., "Thin Layer Approximation and Algebraic Model for Separated Turbulent Flows," AIAA Paper 78-257, Jan. 1978.

[17]He, L., "Method of Simulating Unsteady Turbomachinery Flows with Multiple Perturbations," *AIAA Journal*, Vol. 30, No. 11, 1992, pp. 2730–2735.

[18]Ni, R. H., and Sisto, F., "Numerical Computation of Nonstationary Aerodynamics of Flat Plate Cascade in Compressible Flow," American Society of Mechanical Engineers, ASME Paper 75-GT-5, 1975.

[19]He, L., "New Two-Grid Acceleration Method for Unsteady Navier–Stokes Calculations," *Journal of Propulsion and Power*, Vol. 9, No. 2, 1993, pp. 272–280.

[20]Jameson, A., Schmidt, W., and Turkel, E., "Numerical Solutions of the Euler Equation by Finite Volume Method Using Runge–Kutta Time-Stepping Scheme," AIAA Paper 81-1259, June 1981.

[21]Giles, M. B., "Nonreflecting Boundary Conditions for the Euler Equations," *AIAA Journal*, Vol. 28, No. 12, 1990, pp. 2050–2058.

[22]Denton, J. D., "The Calculation of Three-Dimensional Viscous Flow Through Multistage Turbomachine," American Society of Mechanical Engineers, ASME Paper 90-GT-19, June 1990.

[23]Lighthill, M. J., "The Response of Laminar Skin Friction and Heat Transfer to Fluctuations in the Stream Velocity," *Proceedings of the Royal Society of London*, Vol. A224, 1954, pp. 1–23.

[24]Cebeci, T., "Calculation of Unsteady Two-Dimensional Laminar and Turbulent Boundary Layers with Fluctuations in External Velocity," *Proceedings of Royal Society of London*, Vol. A355, 1977, pp. 225–238.

[25]Karlsson, S. K. F., "An Unsteady Turbulent Boundary Layer," *Journal of Fluid Mechanics*, Vol. 5, 1959, pp. 622–636.

[26]Sajben, M., Bogar, T. J., and Kroutil, J. C., "Forced Oscillation Experiments in Supercritical Diffuser Flows," *AIAA Journal*, Vol. 22, No. 4, 1984, pp. 465–474.

K. Kailasanath
Associate Editor